INTERNATIONAL JOURNAL OF PRECISION ENGINEERING AND MANUFACTURING Vol. 15, No. 12, pp. 2611-2616 DECEMBER 2014 / 2611
DOI: 10.1007/s12541-014-0634-0

Octahedron Pore Architecture to Enhance Flexibility of Nasal Implant-Shaped Scaffold for Rhinoplasty

Jin Woo Jung[1], Jeong Hun Park[1], Jung Min Hong[1], Hyun-Wook Kang[2], and Dong-Woo Cho[1,#]

1 Department of Mechanical Engineering, POSTECH, 77, Cheongam-ro, Nam-gu, Pohang-si, Gyeongsangbuk-do, South Korea, 790-784
2 Wake Forest Institute for Regenerative Medicine, Medical Center Boulevard, Winston-Salem, North Carolina, United States, 27157
Corresponding Author / E-mail: dwcho@postech.ac.kr, TEL: +82-54-279-2171, FAX: +82-54-279-5419

KEYWORDS: Scaffold, Nasal implant, 3D printing technique, Octahedron pore architecture

This study is a part of ongoing research conducted to develop an ideal implant for augmentation rhinoplasty using a combination of cartilage tissue engineering and 3D printing (3DP) techniques. A promising nasal implant-shaped (NIS) scaffold for rhinoplasty should have flexibility similar enough to native cartilage tissue to maintain its mechanical stability after implantation into a nose. In scaffold fabrication using 3DP, the pore pattern or architecture has a significant effect on the mechanical properties of a scaffold. In this study, we proposed octahedron pore architecture inspired by a zigzag spring, which stores more mechanical energy than a simple rod. Therefore, we assumed that the scaffold having octahedron pore architecture is more flexible than one that has the cube or lattice pore architecture that is widely used in tissue engineering based on 3DP. To verify this assumption, scaffolds having octahedron, cube, or lattice pore architecture with the same porosity and same unit cell size were fabricated using projection-based micro-stereolithography and sacrificial molding, and their mechanical behaviors were analyzed using compression and three-point bending tests. Compared to the other pore types, the octahedron pore architecture had superior flexibility, which is beneficial for clinical application of NIS scaffolds.

Manuscript received: February 18, 2014 / Revised: August 13, 2014 / Accepted: August 14, 2014

1. Introduction

Nasal implants are often used in rhinoplasty to restore, reconstruct, or reshape the nose.[1] Autologous cartilage and silicone are the materials most widely used to construct these implant.[1] Autologous cartilage has good biocompatibility and strength, and is therefore the most ideal graft material, but it has the disadvantages of limited availability and donor site morbidity.[2] Silicone implants have neither of these disadvantages, but their mechanical properties differ from those of native cartilage tissue, and can result in complications such as infection and extrusion.[3-5] Also, silicone implants are usually sculpted manually by surgeons during surgery, so their dimensions may not correspond with the desired ones.

One possible method to solve these complications of current rhinoplasty is to combine 3D printing (3DP) and cartilage tissue engineering. 3DP techniques fabricate three-dimensional (3D) free-form structures by stacking layers of two-dimensional (2D) patterns; it is highly effective at fabricating customized nasal implants to meet patients' individual needs.[6-8] For cartilage regeneration in rhinoplasty, the nasal implant is fabricated as a porous scaffold composed of biodegradable polymer. This polymer should have a suitable degradation rate to match a regeneration rate of neocartilage tissue, which should be non-cytotoxic and has the same mechanical properties as the original native cartilage tissue.[9,10] Consequently, use of a nasal implant-shaped (NIS) scaffold fabricated using 3DP techniques may be a promising strategy for nasal augmentation.

Enhancing flexibility of nasal implant in rhinoplasty helps to distribute external force across a larger area to avoid permanent deformation or failure of the nasal implant and reduce damage to adjacent tissue. Scaffold flexibility can be controlled by slecting n appropriate material, but few materials are available for NIS scaffolds, because the materials must be not only biodegradable and biocompatible, but also approved by the U.S. Food and Drug Administration (FDA). Poly-ε-caprolactone (PCL) is the best candidate polymer for NIS scaffolds among the few FDA-approval materials due to its suitable biodegradability. PCL has sufficient biodegradability from several months to a few years, so it can stably supporte an NIS scaffold while neocartilage tissue is fully regenerated. Also, many papaers have reported cartilage tissue regeneration studies using PCL scaffold. However, PCL is too rigid for use as a scaffold for rhinoplasty, and is therefore not suitable for clinical use in NIS scaffolds due to potential

complications such as extrusion. Other biodegradable elastomers with high flexibility are available for only researches, but have not gained FDA approval.[11,12] Therefore, a method is needed that can fabricate a sufficiently flexible scaffold from FDA-approved biodegradable materials.

The flexibility of a scaffold can also be controlled by adjusting its pore architecture.[13,14] Here we report a method for design and fabrication of a scaffold with octahedron pore architecture having high flexibility, which can be used in an NIS scaffold. This architecture resembles the circular pattern of a zigzag spring. An NIS scaffold model having this type pore was generated using an intersection Boolean operation between the external shape of nasal implant and pore architecture.[15,16] The flexibility of this pore type, and the viability of cells living in it, was compared with those of the cube and lattice type pores that have been used in 3DP fabrication of scaffolds for use in tissue engineering.

2. Materials and Methods

2.1 Design of scaffolds and their sacrificial molds

The NIS scaffold was fabricated by using projection-based micro-stereolithography (pMSTL) to construct a mold, injecting biomaterial into it, then removing the mold to leave the scaffold.[14,15] Commercial CAD software (CATIA V5, Dassault Systemes) was used to generate a model of the sacrificial mold for the NIS scaffold after designing the scaffold.

2.1.1 Internal pore architecture design

The octahedron pore architecture was inspired by the zigzag spring, which is more flexible than a simple rod.[17,18] The zigzag spring designed in this study consisted of 0.5-mm diameter struts inclined at 45° to the horizontal. A unit cell octahedron pore was designed with circular pattern to duplicate the unit cell of the zigzag spring as shown in Fig. 1a. The internal pore structure of the scaffold was generated using a rectangular pattern to duplicate its unit cell along three orthogonal directions as presented in Fig. 1b. For comparison of effectiveness, cube and lattice pore architectures were also designed using a similar process.

2.1.2 Design of nasal implant shape

A commercial silicone nasal implant was provided by the Department of Plastic and Reconstructive Surgery (Seoul National University College of Medicine). Shape and size of several cross-sections of the implant were carefully measured using vernier calipers; then the approximate cross-sections were drawn in CATIA in accordance with their relative positions on the real object. The Multi-section Solid tool in CATIA automatically calculated the solid model from these cross-sections as shown in Fig. 2.

2.1.3 Scaffolds and their sacrificial mold design

NIS scaffold (approximately 9.4×8.2×50 mm) models composed of octahedron, cube or lattice pore architectures were generated by the intersection Boolean operation between the nasal implant model and the pore architectures. In the same manner, rectangular scaffold (4×4×4 mm) models with the pore architecture were designed. Subsequently,

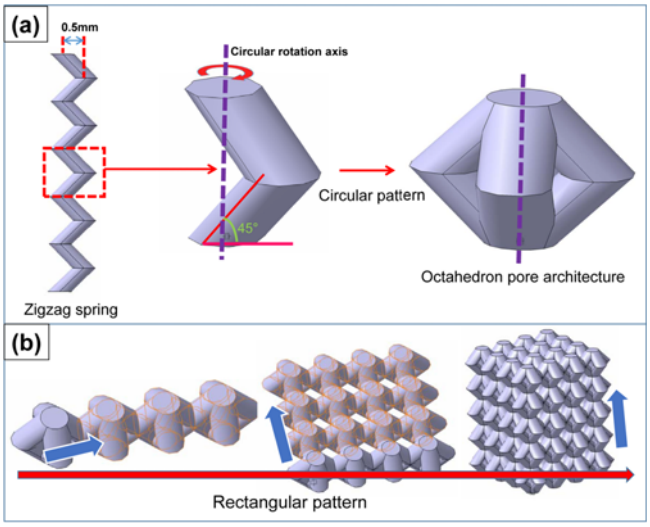

Fig. 1 (a) Design of octahedron pore architecture composed of struts with a diameter of 0.5 mm, inclination angle of 45°, and unit cell size of 1 mm. (b) Internal pore structure design using rectangular pattern of octahedron pore architecture along three orthogonal directions

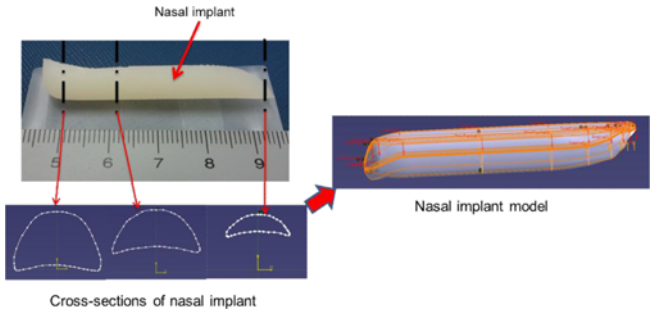

Fig. 2 Nasal implant model design using Multi-section Solid tool

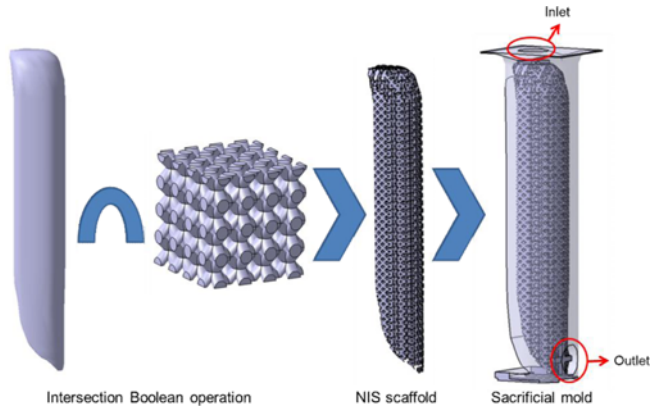

Fig. 3 Scaffold design by internal Boolean operation between external shape, and pore architecture and mold design by removal Boolean operation of scaffold from mold frame

the mold frame was designed according to each scaffold model size. Fig. 3 shows the design of each mold of the scaffold was completed by removing Boolean operation of the scaffold from the mold frame. The

inlets and outlets of the mold models were designed to allow material injection. The mold models were converted to fabrication data for the pMSTL system as described elsewhere.[19]

2.2 Preparation of alkali-soluble photopolymer

The photo-crosslinking polymer for the sacrificial molding process should be quickly dissolved; for this reason, an alkali-soluble photopolymer was synthesized by stirring-induced mixing N,N-dimethyl-acrylamide (Sigma-Aldrich), methacrylic acid (Sigma-Aldrich), Poly(vinyl pyrrolidone) (Sigma-Aldrich, MW: 360,000), Irgacure 819 (Ciba Specialty Chemicals) and 1, 4-dihydroxyanthraquinone (Sigma-Aldrich) in 21:68:11:4:0.3 weight ratio at room temperature (RT).[20-22]

2.3 Fabrication of sacrificial molds using pMSTL system

The sacrificial molds were fabricated using pMSTL, which is a 3DP technique to produce a structure by stacking photo-polymerized 2D patterns.[21,22] A pMSTL system projects an ultra-violet (UV) light beam with a 2D pattern onto a photopolymer resin coated which then solidifies by photo-polymerization into a replica of the pattern. The patterned resin is detached from the substrate and the cycle is repeated successively to stack 2D patterns until the 3D object is fabricated.

2.4 Sacrificial molding process to obtain the scaffolds

Poly-ε-caprolactone (PCL, Polysciences Inc., MW 43,000~50,000) was dissolved in chloroform (1.5:1 w:v) then injected through the inlet of the sacrificial molds using a 1 mm plastic syringe. The sacrificial molds were immersed in isopropyl alcohol to solidify the PCL/chloroform solution by removing the chloroform, then the molds were fully dissolved in 0.5 M NaOH solution to obtain the scaffolds. Residual NaOH was removed by washing the scaffolds several times in distilled water.

2.5 Scanning Electron Microscopy

The scaffolds were dried in vacuum at RT for about 4 h, then sputter-coated with platinum. Their morphologies were observed using a scanning electron microscope (SU-6600, Hitachi) at an accelerating voltage of 15 kV.

2.6 Mechanical behavior test

The elastic modulus and bending behavior of each scaffold model were analyzed using a compression test and a three-point bending test, respectively using a single column testing system (Instron 3340, Instron). These tests were conducted in the wet state at RT.

For the compressive test, each rectangular scaffold was placed on a stainless steel flat plate, and the stress-strain curve was obtained by applying a load at a crosshead speed of 0.5 mm/min. The elastic modulus was calculated from the initial linear region of the curve.

For the three-point bending test, the two end points of an NIS scaffold were mounted horizontally on the gripping units of the testing device, and shear force was directed vertically to the middle point of scaffold. Fig. 4 presents the three-point bending test of an NIS scaffold. The reaction force-deflection curve was recorded at a crosshead speed of 0.5 mm/min until the scaffold broke. The deflection at the time of breakage was defined as the deflection at the moment when the highest reaction force occurred on the curve.

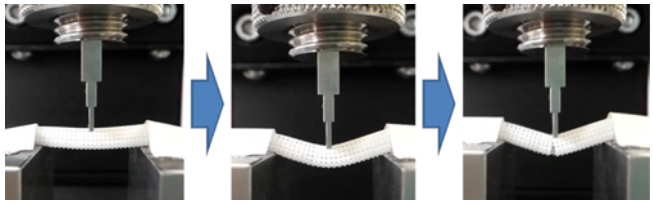

Fig. 4 Three-point bending test of an NIS scaffold with octahedron pore architecture

2.7 Cell seeding and *in vitro* culture

Human chondrocytes (C-20/A4) were cultured in Dulbecco's modified Eagle's medium/Ham's F-12 medium (Gibco-BRL) supplemented with 10% bovine serum (Gibco-BRL) and 1% penicillin/streptomycin (Gibco-BRL) at 37°C in a humidified atmosphere of 5% CO_2.[20] Before being seeded with cells, all NIS scaffolds were sterilized by UV irradiation and immersion in 70% ethanol. C-20/A4 cell lines were seeded (2×10^4 cells/scaffold) onto the scaffolds. The culture medium was changed every two days.

2.8 Cell viability assay

The cell viability on scaffolds was evaluated using a Cell Count Kit-8 (CCK-8, Dojindo Molecular Technology) after cultivation in 1, 4, and 7 day to quantify cell attachment and proliferation rate on the scaffold. Specimens were incubated with 200 μL medium and 20 μL CCK-8 solution for 2 h at 37°C. Absorbance was determined at 490 nm using a microplate reader (Wallac 1420; Perkin Elmer).

2.9 Statistical analysis

The results of each compressive test and three-point bending test are reported as mean±standard deviation (SD) for n=4. Cell viability was assessed through biochemical assay to measure the number of viable cells in media with n=4. The results are reported as mean±SD. The statistical significance (p<0.05) levels between experimental groups were determined using one-way Analysis of variance (ANOVA).

3. Result and Discussion

3.1 Design of scaffolds and their sacrificial molds

The scaffolds and their mold models were designed using commercial CAD/CAM software, CATIA (Dassault Systèmes). Briefly, internal pore architecture and external structure were individually designed, then their geometrical information was merged using an intersection Boolean operation to generate a scaffold structure. The molds of the scaffold were designed using a removal Boolean operation between scaffold model and mold frame. This scaffold design process using Boolean operation allows the scaffold and mold design process to be simplified by using pre-developed libraries of scaffold internal structure, anatomical shape, and mold frame.[15,16] By this process, the NIS and regular scaffolds having each of octahedron, cube, and lattice pore architectures and the sacrificial molds of the scaffolds were designed. As represented in Fig. 5, these scaffolds share the similar porosity (approximately 50%) and the same unit cell size (1 mm). The designed mold model was exported into the STL file format, which was subsequently converted to pixel-

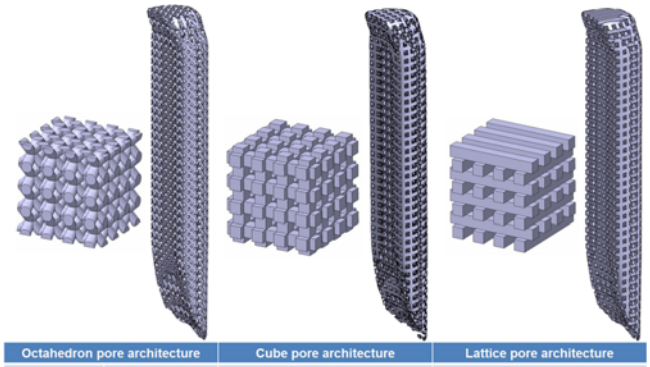

Octahedron pore architecture		Cube pore architecture	Lattice pore architecture
Porosity	50.07%	50%	50%
Unit cell size	1 mm	1 mm	1 mm
Strut size	500 μm diameter	500 μm length	500 μm thickness

Fig. 5 NIS scaffold and regular scaffold having each of octahedron (left), cube (middle), and lattice (right) pore architectures with similar porosity and same unit cell size (bottom)

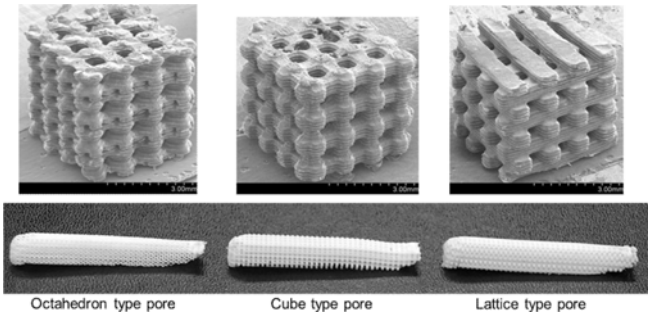

Fig. 6 SEM images of the rectangular scaffolds (upper), and picture images of the NIS scaffolds (lower)

based data for 3DP using pMSTL.[19] Fig. 6 represents that fabrication of the molds for NIS scaffold and regular scaffold was achieved by vertically stacking cross-section layers of the mold. The scaffold surfaces were not smooth, but showed a stair-stepping structure as a natural result of the process of stacking layers.[23] Similar surface pattern or roughness occurs on each scaffolds regardless of their pore architecture, because the scaffolds were fabricated by same manufacturing procedures including 3D printing and injection molding. Similar surface patterns or roughnesses can be assumed to have similar effects on the mechanical behavior of the scaffolds. Thus, although the surface roughness of the scaffold could influence the mechanical characteristics, including flexibility, it is only weakly related to the effect of pore architecture on mechanical characteristics or flexibility.

3.2 Compressive and bending behavior

The analysis of the effect of the pore architecture on the mechanical behavior of the scaffold was conducted using a compression test and a three-point bending test. We recorded the compressive response of the scaffolds with octahedron, cube, and lattice pore architectures at similar porosity, and calculated their elastic modulus. As shown in Fig. 7, the elastic modulus (4.8585±1.1079 MPa) of the octahedron pore architecture derived from compression test was lower than those of the cube (7.6581±0.1505 MPa) and lattice pore architecture (12.6038±

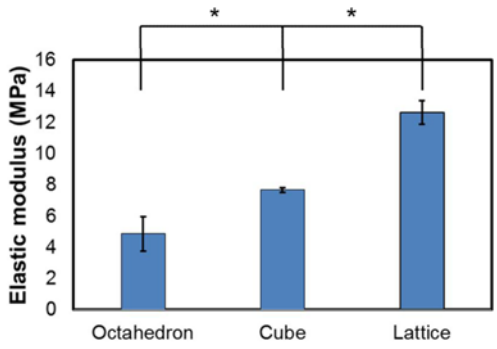

Fig. 7 Elastic modulus calculated from stress-strain curves of scaffolds with octahedron, cube and lattice type pore in compression test (*p< 0.05)

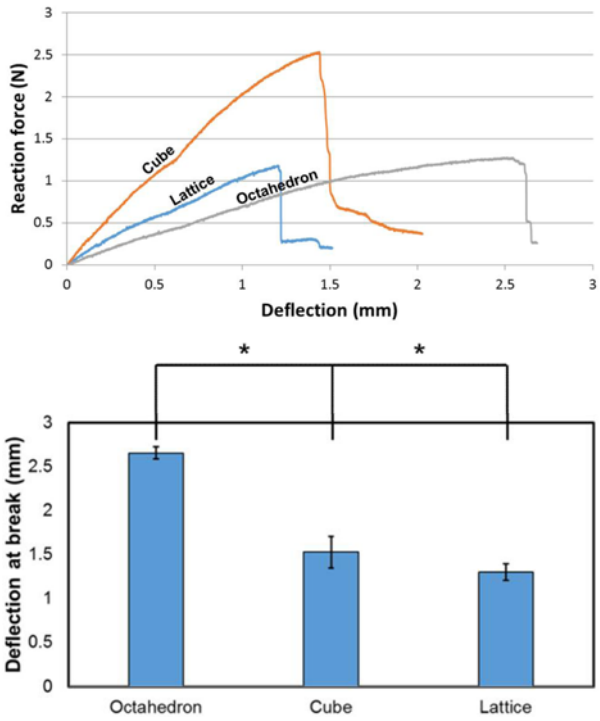

Fig. 8 Reaction force-deflection curve (top) of NIS scaffolds in three-point bending test and the deflection at break (bottom) measured from the curve (*p<0.05)

0.7564 MPa). Fig. 8 shows the bending behavior was determined for each scaffold. The bending deflection at break indicates that the octahedron pore architecture (2.6543±0.0669 mm) is relatively more pliable than cube (1.5269±0.1780 mm) and lattice (1.3018±0.0919 mm) pore architectures. As shown in Fig. 8, the slopes in the reaction force-deflection curve indicate the flexibility of the pore architectures; these results demonstrate that the octahedron pore architecture makes the NIS scaffold softer and more flexible under deformation than the other structures within surrounding nasal tissues. Such benefits result in decreasing damage to surrounding tissues and reduced possibility of rupture of the NIS, scaffold when an external force is applied to the nose. In this regard, we consider that octahedron pore architecture has more suitable mechanical properties for rhinoplasty based on the NIS

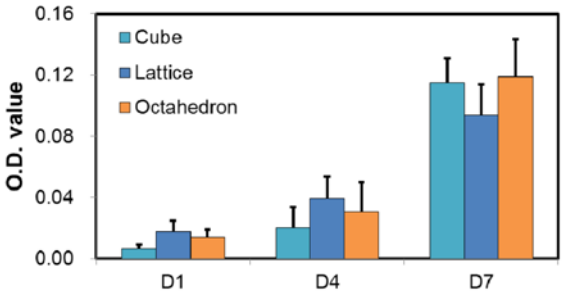

Fig. 9 Cell attachment on scaffolds with octahedron, cube, and lattice pore architectures. C-20/A4 cell lines were cultured on the scaffolds at days (D) 1, 4, and 7

scaffold than do cube or lattice pore architecture.

3.3 Cell viability

Cell proliferation rates did not differ significantly (one-way ANOVA, $p>0.05$) among scaffold types for 7 days after culture as shown in Fig. 9; therefore, the octahedron pore architecture had no disadvantage in cell viability, such as attachment and proliferation, compared to the cube and lattice pore architectures, and is acceptable for use in tissue engineering.

4. Conclusions

Many studies have been undertaken to develop or improve a material to control or enhance the mechanical properties of a scaffold. However, approval to use a new biomaterial for clinical application is very difficult to obtain due to a strict and prolonged process for evaluating whether the material is completely biocompatible in the body. Because the final goal of this study is to develop a nasal implant-shaped scaffold for clinical application in rhinoplasty, a clinically-approved biodegradable material should be considered as scaffold material. A few biodegradable materials have been approved by the FDA, such as poly (ε-caprolactone), poly (lactic acid), poly (glycolic acid), poly (lactic-co-glycolic acid), and poly (ethylene glycol).[24-26] NIS scaffolds composed of these materials should be at least as flexible as a nasal silicone implant to avoid complications such as extrusion. However, these materials cannot be as flexible as silicone which has an unacceptably high complication rate in rhinoplasty.[2] Although only a few material factors such as molecular weight (MW) can be exploited to for manipulate mechanical properties without changing chemical composition, enhancing flexibility by changing the MW leads to increase of rigidity.[27] Use of a rigid NIS scaffold for rhinoplasty could result in complications such as extrusion and infection. Therefore, we suggest that the flexibility of a scaffold should be increased by methods that are independent of the materials used. The pore architecture of a scaffold can have significant effects on its mechanical properties.[28] In this regard, we suggested the use of octahedron pore architecture for clinical application of biodegradable NIS scaffolds in rhinoplasty and verified that the octahedron structure is more flexible than cube and lattice pore architectures, which have been widely used for tissue engineering based on 3DP. From the results, octahedron pore architecture could be expected to improve the mechanical behavior of scaffolds for engineering of other soft tissues such as liver, fat, and muscle.

ACKNOWLEDGEMENT

This work was supported by the National Research Foundation of Korea (NRF) grant funded by the Korea government (MSIP) (No. 2010-0018294).

REFERENCES

1. Vuyk, H. D. and Adamson, P. A., "Biomaterials in Rhinoplasty," Clinical Otolaryngology, Vol. 23, No.3, pp. 209-217, 1998.
2. Lin, G. and Lawson, W., "Complications using Grafts and Implants in Rhinoplasty," Operative Techniques in Otolaryngology-Head and Neck Surgery, Vol. 18, No. 4, pp. 315-323, 2007.
3. Hutmacher, D. W., Schantz, T., Zein, I., Ng, K. W., Teoh, S. H., and Tan, K. C., "Mechanical Properties and Cell Cultural Response of Polycaprolactone Scaffolds Designed and Fabricated Via Fused Deposition Modeling," Journal of Biomedical Materials Research, Vol. 55, No. 2, pp. 203-216, 2001.
4. Zein, I., Hutmacher, D. W., Tan, K. C., and Teoh, S. H., "Fused Deposition Modeling of Novel Scaffold Architectures for Tissue Engineering Applications," Biomaterials, Vol. 23, No. 4, pp. 1169-1185, 2002.
5. Tham, C., Lai, Y. L., Weng, C. J., and Chen, Y. R., "Silicone Augmentation Rhinoplasty in an Oriental Population," Annals of Plastic Surgery, Vol. 54, No. 1, pp. 1-5, 2005.
6. Seol, Y. J., Kang, T. Y., and Cho, D. W., "Solid Freeform Fabrication Technology Applied to Tissue Engineering with Various Biomaterials," Soft Matter, Vol. 8, No. 6, pp. 1730-1735, 2012.
7. Sohn, Y. S., Jung, J. W., Kim, J. Y., and Cho, D. W., "Investigation of Bi-Pore Scaffold based on the Cell Behaviors on 3D Scaffold Patterns," Tissue Engineering and Regenerative Medicine, Vol. 8, No. 4, pp. 66-72, 2011.
8. Ciocca, L., De Crescenzio, F., Fantini, M., and Scotti, R., "CAD/CAM and Rapid Prototyped Scaffold Construction for Bone Regenerative Medicine and Surgical Transfer of Virtual Planning: A Pilot Study," Computerized Medical Imaging and Graphics, Vol. 33, No. 1, pp. 58-62, 2009.
9. Huey, D. J., Hu, J. C., and Athanasiou, K. A., "Unlike Bone, Cartilage Regeneration Remains Elusive," Science, Vol. 338, No. 6109, pp. 917-921, 2012.
10. Xia, W., Liu, W., Cui, L., Liu, Y., Zhong, W., et al., "Tissue Engineering of Cartilage with the Use of ChitosanGelatin Complex Scaffolds," Journal of Biomedical Materials Research Part B: Applied Biomaterials, Vol. 71, No. 2, pp. 373-380, 2004.

11. Wang, Y., Ameer, G. A., Sheppard, B. J., and Langer, R., "A Tough Biodegradable Elastomer," Nature Biotechnology, Vol. 20, No. 6, pp. 602-606, 2002.

12. Jung, Y., Park, M. S., Lee, J. W., Kim, Y. H., Kim, S. H., and Kim, S. H., "Cartilage Regeneration with Highly-Elastic Three-Dimensional Scaffolds Prepared from Biodegradable Poly (L-Lactide-Co--Caprolactone)," Biomaterials, Vol. 29, No. 35, pp. 4630-4636, 2008.

13. Lee, J. S., Cha, H. D., Shim, J. H., Jung, J. W., Kim, J. Y., and Cho, D. W., "Effect of Pore Architecture and Stacking Direction on Mechanical Properties of Solid Freeform Fabricationbased Scaffold for Bone Tissue Engineering," Journal of Biomedical Materials Research Part A, Vol. 100, No. 7, pp. 1846-1853, 2012.

14. Kang, H. W., Park, J. H., Kang, T. Y., Seol, Y. J., and Cho, D. W., "Unit Cell-based Computer-Aided Manufacturing System for Tissue Engineering," Biofabrication, Vol. 4, No. 1, Paper No. 015005, 2012.

15. Yoo, D. J., "Porous Scaffold Design using the Distance Field and Triply Periodic Minimal Surface Models," Biomaterials, Vol. 32, No. 31, pp. 7741-7754, 2011.

16. Sun, W., Starly, B., Nam, J., and Darling, A., "Bio-CAD Modeling and Its Applications in Computer-Aided Tissue Engineering," Computer-Aided Design, Vol. 37, No. 11, pp. 1097-1114, 2005.

17. Komatsubara, M., Namazu, T., Nagasawa, H., Tsurui, T., and Inoue, S., "Cylindrical Film Deposition System for Three-Dimensional Titanium-Nickel Shape Memory Alloy Microstructure," Vacuum, Vol. 83, No. 3, pp. 703-707, 2008.

18. Tawney, G. L., "Zigzag and Helical Springs; Elastic Properties of Molybdenum," Review of Scientific Instruments, Vol. 10, No. 5, pp. 152-159, 1939.

19. Jung, J. W., Kang, H. W., Kang, T. Y., Park, J. H., Park, J., and Cho, D.-W., "Projection Image-Generation Algorithm for Fabrication of a Complex Structure using Projection-based Microstereolithography," Int. J. Precis. Eng. Manuf., Vol. 13, No. 3, pp. 445-449, 2012.

20. Liska, R., Schwager, F., Maier, C., CanoVives, R., and Stampfl, J., "WaterSoluble Photopolymers for Rapid Prototyping of Cellular Materials," Journal of Applied Polymer Science, Vol. 97, No. 6, pp. 2286-2298, 2005.

21. Kang, H. W. and Cho, D. W., "Development of an Indirect Stereolithography Technology for Scaffold Fabrication with a Wide Range of Biomaterial Selectivity," Tissue Engineering Part C: Methods, Vol. 18, No. 9, pp. 719-729, 2012.

22. Kang, H. W., Seol, Y. J., and Cho, D. W., "Development of an Indirect Solid Freeform Fabrication Process based on Microstereolithography for 3D Porous Scaffolds," Journal of Micromechanics and Microengineering, Vol. 19, No. 1, Paper No. 015011, 2009.

23. Pan, Y., Zhao, X., Zhou, C., and Chen, Y., "Smooth Surface Fabrication in Mask Projection based Stereolithography," Journal of Manufacturing Processes, Vol. 14, No. 4, pp. 460-470, 2012.

24. Atala, A. and Mooney, D. J., "Synthetic Biodegradable Polymer Scaffolds," Springer, pp. 1-12, 1997.

25. Neuendorf, R. E., Saiz, E., Tomsia, A. P., and Ritchie, R. O., "Adhesion between Biodegradable Polymers and Hydroxyapatite: Relevance to Synthetic Bone-like Materials and Tissue Engineering Scaffolds," Acta Biomaterialia, Vol. 4, No. 5, pp. 1288-1296, 2008.

26. Lutz, J. F. and Hoth, A., "Preparation of Ideal Peg Analogues with a Tunable Thermosensitivity by Controlled Radical Copolymerization of 2-(2-Methoxyethoxy) Ethyl Methacrylate and Oligo (ethylene glycol) Methacrylate," Macromolecules, Vol. 39, No. 2, pp. 893-896, 2006.

27. Nguyen, T. Q. and Kausch, H. H., "Molecular Weight Distribution and Mechanical Properties," Mechanical Properties and Testing of Polymers, Vol. 3, pp. 143-150, 1999.

28. Melchels, F. P., Bertoldi, K., Gabbrielli, R., Velders, A. H., Feijen, J., and Grijpma, D. W., "Mathematically Defined Tissue Engineering Scaffold Architectures Prepared by Stereolithography," Biomaterials, Vol. 31, No. 27, pp. 6909-6916, 2010.